

# Simultaneous multi-frequency observation of the unknown redshift blazar PG 1553+113 in March-April 2008

J. Aleksić<sup>1</sup>, H. Anderhub<sup>2</sup>, L. A. Antonelli<sup>3</sup>, P. Antoranz<sup>4</sup>, M. Backes<sup>5</sup>, C. Baixeras<sup>6</sup>, S. Balestra<sup>4</sup>, J. A. Barrio<sup>4</sup>, D. Bastieri<sup>7</sup>, J. Becerra González<sup>8</sup>, J. K. Becker<sup>5</sup>, W. Bednarek<sup>9</sup>, A. Berdyugin<sup>10</sup>, K. Berger<sup>9</sup>, E. Bernardini<sup>11</sup>, A. Biland<sup>2</sup>, R. K. Bock<sup>12,7</sup>, G. Bonnoli<sup>13</sup>, P. Bordas<sup>14</sup>, D. Borla Tridon<sup>12</sup>, V. Bosch-Ramon<sup>14</sup>, D. Bose<sup>4</sup>, I. Braun<sup>2</sup>, T. Bretz<sup>15</sup>, D. Britzger<sup>12</sup>, M. Camara<sup>4</sup>, E. Carmona<sup>12</sup>, A. Carosi<sup>3</sup>, P. Colin<sup>12</sup>, S. Commichau<sup>2</sup>, J. L. Contreras<sup>4</sup>, J. Cortina<sup>1</sup>, M. T. Costado<sup>8,16</sup>, S. Covino<sup>3</sup>, F. Dazzi<sup>17,26</sup>, A. De Angelis<sup>17</sup>, E. de Cea del Pozo<sup>18</sup>, R. De los Reyes<sup>4,28</sup>, B. De Lotto<sup>17</sup>, M. De Maria<sup>17</sup>, F. De Sabata<sup>17</sup>, C. Delgado Mendez<sup>8,27</sup>, A. Domínguez<sup>19</sup>, D. Dominis Prester<sup>20</sup>, D. Dorner<sup>2</sup>, M. Doro<sup>7</sup>, D. Elsaesser<sup>15</sup>, M. Errando<sup>1</sup>, D. Ferenc<sup>21</sup>, E. Fernández<sup>1</sup>, R. Firpo<sup>1</sup>, M. V. Fonseca<sup>4</sup>, L. Font<sup>6</sup>, N. Galante<sup>12</sup>, R. J. García López<sup>8,16</sup>, M. Garczarczyk<sup>1</sup>, M. Gaug<sup>8</sup>, N. Godinovic<sup>20</sup>, F. Goebel<sup>12,29</sup>, D. Hadasch<sup>18</sup>, A. Herrero<sup>8,16</sup>, D. Hildebrand<sup>2</sup>, D. Höhne-Mönch<sup>15</sup>, J. Hose<sup>12</sup>, D. Hrupec<sup>20</sup>, C. C. Hsu<sup>12</sup>, T. Jogler<sup>12</sup>, S. Klepser<sup>1</sup>, T. Krähenbühl<sup>2</sup>, D. Kranich<sup>2</sup>, A. La Barbera<sup>3</sup>, A. Laille<sup>21</sup>, E. Leonardo<sup>13</sup>, E. Lindfors<sup>10</sup>, S. Lombardi<sup>7</sup>, F. Longo<sup>17</sup>, M. López<sup>7</sup>, E. Lorenz<sup>2,12</sup>, P. Majumdar<sup>11</sup>, G. Maneva<sup>22</sup>, N. Mankuzhiyil<sup>17</sup>, K. Mannheim<sup>15</sup>, L. Maraschi<sup>3</sup>, M. Mariotti<sup>7</sup>, M. Martínez<sup>1</sup>, D. Mazin<sup>1</sup>, M. Meucci<sup>13</sup>, J. M. Miranda<sup>4</sup>, R. Mirzoyan<sup>12</sup>, H. Miyamoto<sup>12</sup>, J. Moldón<sup>14</sup>, M. Moles<sup>19</sup>, A. Moralejo<sup>1</sup>, D. Nieto<sup>4</sup>, K. Nilsson<sup>10</sup>, J. Ninkovic<sup>12</sup>, R. Orito<sup>12</sup>, I. Oya<sup>4</sup>, R. Paoletti<sup>13</sup>, J. M. Paredes<sup>14</sup>, M. Pasanen<sup>10</sup>, D. Pascoli<sup>7</sup>, F. Pauss<sup>2</sup>, R. G. Pegna<sup>13</sup>, M. A. Perez-Torres<sup>19</sup>, M. Persic<sup>17,23</sup>, L. Peruzzo<sup>7</sup>, F. Prada<sup>19</sup>, E. Prandini<sup>7</sup>, N. Puchades<sup>1</sup>, I. Puljak<sup>20</sup>, I. Reichardt<sup>1</sup>, W. Rhode<sup>5</sup>, M. Ribó<sup>14</sup>, J. Rico<sup>24,1</sup>, M. Rissi<sup>2</sup>, S. Rügamer<sup>15</sup>, A. Saggion<sup>7</sup>, T. Y. Saito<sup>12</sup>, M. Salvati<sup>3</sup>, M. Sánchez-Conde<sup>19</sup>, K. Satalecka<sup>11</sup>, V. Scalzotto<sup>7</sup>, V. Scapin<sup>17</sup>, T. Schweizer<sup>12</sup>, M. Shayduk<sup>12</sup>, S. N. Shore<sup>25</sup>, A. Sierpowska-Bartosik<sup>9</sup>, A. Sillanpää<sup>10</sup>, J. Sitarek<sup>12,9</sup>, D. Sobczynska<sup>9</sup>, F. Spanier<sup>15</sup>, S. Spiro<sup>3</sup>, A. Stamerra<sup>13</sup>, B. Steinke<sup>12</sup>, N. Strah<sup>5</sup>, J. C. Strüebig<sup>15</sup>, T. Suric<sup>20</sup>, L. Takalo<sup>10</sup>, F. Tavecchio<sup>3</sup>, P. Temnikov<sup>22</sup>, D. Tescaro<sup>1</sup>, M. Teshima<sup>12</sup>, D. F. Torres<sup>24,18</sup>, N. Turini<sup>13</sup>, H. Vankov<sup>22</sup>, R. M. Wagner<sup>12</sup>, V. Zabalza<sup>14</sup>, F. Zandanel<sup>19</sup>, R. Zanin<sup>1</sup>, J. Zapatero<sup>6</sup>  
(The MAGIC Collaboration)  
E. Pian<sup>33,39</sup>, V. Bianchin<sup>30</sup>, F. D'Ammando<sup>31</sup>, G. Di Cocco<sup>30</sup>, D. Fugazza<sup>32</sup>, G. Ghisellini<sup>32</sup>, O. M. Kurtanidze<sup>38</sup>, C. M. Raiteri<sup>34</sup>, G. Tosti<sup>35</sup>, A. Treves<sup>36</sup>, S. Vercellone<sup>37</sup>, and M. Villata<sup>34</sup>

(Affiliations can be found after the references)

Received .....; accepted .....

## ABSTRACT

The blazar PG 1553+113 is a well known TeV  $\gamma$ -ray emitter. In this paper, we determine its spectral energy distribution using simultaneous multi-frequency data in order to study its emission processes. An extensive campaign was carried out between March and April 2008, where optical, X-ray, high-energy (HE)  $\gamma$ -ray, and very-high-energy (VHE)  $\gamma$ -ray data were obtained with the KVA, Abastumani, REM, RossiXTE/ASM, AGILE and MAGIC telescopes, respectively. This is the first simultaneous broad-band (i.e., HE+VHE)  $\gamma$ -ray observation, though AGILE did not detect the source. We combine data to derive source's spectral energy distribution and interpret its double peaked shape within the framework of a synchrotron self compton model.

**Key words.** BL Lacertae objects: individual: PG 1553+113 - Gamma rays: observation - Gamma rays: theory

## 1. Introduction

The transformation of gravitational energy in an accretion disk around a supermassive black hole into radiation is the widely believed underlying cause of emission in active galactic nuclei (AGN). Furthermore, the emission is beamed from jet, perpendicular to the disk by a mechanism that, although not fully understood yet, most likely relates to the focusing properties of the rotating, fully ionized accretion disk (e.g. Blandford & Znajek 1977). The viewing angle of the observer determines the ob-

served phenomenology of AGN (Urry & Padovani 1995). The AGN whose relativistic plasma jets point towards the observer are called blazars. The blazar class includes Flat Spectrum Radio Quasars (FSRQs) and BL Lac objects, the main difference between the two classes is in their emission lines, which are strong and quasar-like for FSRQs and weak or absent in BL Lacs.

The overall (radio to  $\gamma$ -ray) spectral energy distribution (SED) of blazars shows two broad non-thermal continuum peaks. For high peaked BL Lac objects (HBLs), the first peak of the SED is in the UV/X-ray bands [as opposed to IR/optical for low peaked BL Lac objects, LBLs] whereas the second peak is in multi GeV band (multi MeV for LBLs). The low energy peak

is thought to arise from electron synchrotron emission. The leptonic model suggests that the second peak forms due to inverse Compton emission. This can be due to scattering the synchrotron photons by the non-thermal population of electrons responsible for the synchrotron radiation (Synchrotron Self Compton, SSC; eg: Maraschi 1992) or of photons that originate outside the relativistic plasma blob (External Compton, EC; an external source of such ‘seed’ photons could be the accretion disk (eg: Dermer 1993) and/or the broadline region (eg: Sikora et al. 1994)). Blazars often show violent flux variability, that may or may not be correlated between the different energy bands. Strictly simultaneous observations are crucial to investigate these correlations and understand the underlying physics of blazars.

The HBL source PG 1553+113 was firmly detected at very high energy  $\gamma$ -rays (VHE; photon energy  $E > 100$  GeV) by MAGIC at a significance level of  $8.8\sigma$  above 200 GeV, based on data from April - May 2005 and January - April 2006 (Albert et al. 2007). Observations with the H.E.S.S. telescope array in 2005 yielded a tentative detection in VHE band, at the level of  $4\sigma$  ( $5.3\sigma$  using a low energy threshold analysis; Aharonian et al. 2006), which was confirmed later with the combination of the 2005 and 2006 datasets (Aharonian et al. 2008). After the first detection of PG 1553+113 with MAGIC, a multi-frequency campaign on this source was conducted in July 2006 (Albert et al. 2009). The main difference between our present and previous campaign is the use of X-ray and the high energy (HE; photon energy  $E > 100$  MeV) flux.

The lack of detection of spectral lines (neither in emission nor in absorption) in the optical spectrum of PG 1553+113 makes it impossible to measure its redshift directly (Falomo & Treves 1990). However, an ESO-VLT spectroscopic survey of unknown-redshift BL Lac objects suggests  $z > 0.09$  (Sbarufatti et al. 2006), while the absence of host galaxy detection in HST images raises this lower limit to  $z > 0.25$  (Treves et al. 2007). On the other hand, the absence of a break in the VHE spectrum can be interpreted as suggesting  $z < 0.42$  (Mazin & Goebel 2007). The absence of Ly- $\alpha$  forest (Falomo & Treves) in the spectrum also constrains a lower redshift.

## 2. Optical and Near Infrared (NIR) data

### 2.1. KVA observations

The KVA (Kungliga Vetenskaps Akademien, Royal Swedish Academy of Sciences) telescope is located at the Roque de los Muchachos, in the North-Atlantic canary islands of La Palma and is operated by the Tuorla Observatory. The telescope is composed of a 0.6m f/15 Cassegrain devoted to polarimetry, and a 0.35m f/11 SCT auxiliary telescope for multicolour photometry. This telescope has been successfully operated remotely since autumn 2003. The KVA is used for optical (R-band) support observations during MAGIC observations. Typically, one measurement per night and per source is conducted. Photometric measurements are made in differential mode, i.e. by obtaining CCD images of the target and calibrated comparison stars in the same field of view (Fiorucci & Tosti 1996; Fiorucci et al. 1998; Villata et al. 1998).

### 2.2. Abastumani observations

Observations at the Abastumani Observatory (Georgia, FSU) were performed with the 70 cm meniscus telescope (f/3). This is equipped with an Apogee Ap6E CCD camera, with  $390 \times 390$  pixels, and a field of view of  $15 \times 15$  arcmin. Its quantum ef-

iciency is 40% at 4000 Å and 65% at 6750 Å. The frames were acquired in the Cousins’  $R$  band and were reduced with the DAOPHOT II package<sup>1</sup>.

The source magnitude was derived from differential photometry with respect to a reference star in the same field, which lies  $\sim 46$  arcsec east and  $\sim 5$  arcsec south of PG 1553+113. According to the USNO 2.0 Catalogue (Monet et al. 1998), its magnitude is  $R = 13.2$ .

### 2.3. REM observations

REM (Rapid Eye Mount, a fast-slewing robotized infrared telescope; Covino et al. 2001) acquired photometry of PG 1553+113 on April 18, 25 and May 2 2008 with all available filters (VRIJHK). The data reduction followed standard procedures (see e.g. Dolcini et al. 2005). The mean flux of observation is reported in Table 3. The NIR magnitudes were calibrated against the 2MASS catalog. For the SED reconstruction, all magnitudes have been dereddened with the dust IR maps (Schlegel et al. 1998).

## 3. X-rays: RXTE/ASM Observations

The All Sky Monitor (ASM) on board the *Rossi X-ray Timing Explorer* (RXTE) satellite consists of three wide angle scanning shadow cameras. The cameras, mounted on a rotating drive assembly can cover almost 70% of the sky every 1.5 hours (Levine et al. 1996). The measurements were done between March 1 and May 31, 2008. The mean measured flux of PG 1553+113 is shown in table 3.

## 4. $\gamma$ -ray data

### 4.1. HE band: AGILE observations

The Gamma-ray Imaging Detector (GRID, 30 MeV - 30 GeV) on board the high energy astrophysics satellite AGILE (Astro-rivelatore Gamma a Immagini LEggero; Tavani et al. 2009) observed PG 1553+113 in three different time intervals: March 16-21, March 25-30 and April 10-30 2008. The GRID data were analyzed using the AGILE standard pipeline (see Vercellone et al. 2008 for a detailed description of the AGILE data reduction), with a bin size of  $0.25^\circ \times 0.25^\circ$  for  $E > 100$  MeV. Only events flagged as confirmed  $\gamma$ -rays and not recorded while the satellite crossed the South Atlantic Anomaly were accepted. We also rejected all events with a reconstructed direction within  $10^\circ$  from the Earth limb, thus reducing contamination from Earth’s  $\gamma$ -ray albedo. PG 1553+113, observed at about 50 degrees off-axis with respect to the boresight, was not detected by the GRID at a significance level  $> 3\sigma$  and therefore the 95% confidence level upper limit was calculated. Considering that AGILE has a higher particle background at very high off-axis angles, we calculated also the upper limit selecting only photons with energies greater than 200 MeV in order to minimize the possible contamination at low energies. The log of the AGILE observations and the results of the analysis are reported in Table 2. During March - April 2008, the source was outside the field of view of SuperAGILE, the hard X-ray (20-60 keV) imager onboard AGILE (Feroci et al. 2007).

<sup>1</sup> <http://www.star.bris.ac.uk/~mbt/daophot/>

#### 4.2. VHE band: MAGIC observations

The MAGIC Telescope (Baixeras et al. 2004, Cortina et al. 2005) is the most recent generation Imaging Atmospheric Cherenkov Telescope (IACT) at La Palma, Canary Islands, Spain (28.3°N, 17.8°W, 2240 m a.s.l.). Thanks to its low trigger threshold of 50 GeV (25 GeV with a special trigger set up; Albert et al. 2008a), MAGIC is well suited for multi-frequency observations, together with the instruments operating in the GeV range. The parabolic mirror dish with a total mirror area of 236 m<sup>2</sup>, allows MAGIC to collect Cherenkov light from particle showers initiated by  $\gamma$ -rays or other particles in the atmosphere. This Cherenkov light is focused onto a multi-pixel camera composed of 577 ultra-sensitive photomultipliers. The total field of view of the camera is 3.5°. The incident light pulses are converted into optical signals and transmitted via optical fiber to a two-level trigger system. The selected events are digitized by 2 GHz Flash ADCs (Goebel et al. 2007). With a statistical analysis of the recorded light distribution and the orientation of the shower image in the camera, the energy of the primary particle and its incoming direction are reconstructed.

The MAGIC observations for this campaign were carried out on March 16-18 and April 13, 28-30 in 2008. The zenith angle of the data set ranges from 18 degree to 36 degree. Observations were performed in wobble mode (Fomin et al. 1994), where the object was observed at 0.4 degree offset from the camera center in opposite directions every 20 minutes. After data rejection based on the standard quality cuts and the trigger rate, 7.18 hours of total effective observation time data was selected.

An automatic analysis pipeline (Dorner et al., 2005, Bretz & Dorner, 2008) was used to process the data, which includes the muon calibration (Goebel et al. 2005), and an absolute mispointing correction (Riegel et al. 2005). The charge distribution and arrival time information of the pulses of neighboring pixels was used to suppress the contribution from the night sky background in the shower images (Aliu et al. 2009). Three OFF regions were used to determine the background, providing a scaling factor of 1/3 for the background calculation. The shape and orientation of the shower images were used to discriminate  $\gamma$ -like events from the overwhelming background. To select the  $\gamma$ -like events a dynamical cut in Area (Area= $\pi \cdot \text{WIDTH} \cdot \text{LENGTH}$ ) versus SIZE (total charge contained in an image) and a cut in  $\vartheta$  (angular distance between real source position and reconstructed source position) were applied. More details on the cuts can be found in Riegel & Bretz (2005), and the above mentioned image parameters are described by Hillas (1985). The reconstructed  $\gamma$ -ray spectrum is shown in Fig.1. For the spectral reconstruction, looser cuts were applied to ensure that more than 90% of the simulated gamma photons survived. Varying cut efficiencies between 50% and 95% over the entire energy range were applied to the data in order to check systematic effects of the cut efficiency on the spectral shape (shown as gray area in Fig.1). Data which has been affected by calima (sand dust from the Sahara in an air layer between 1.5 km and 5.5 km a.s.l. causing absorption of the Cherenkov light) has been corrected following the method described in Dorner et al. (2009).

## 5. Results and Discussion

Analyzing the MAGIC data, an excess of 415  $\gamma$ -like events, over 1835 normalized background events was found, yielding a significance of  $8.0\sigma$ . The resulting differential VHE spectrum of PG 1553+113, averaged over all observing intervals, is plotted in Fig.1 (filled circles). It can be well described by a power law

Observation period	$F_0$ [ph TeV <sup>-1</sup> s <sup>-1</sup> m <sup>-2</sup> ]	$\Gamma$
March-April 2008	$2.0 \pm 0.3 \times 10^{-6}$	$-3.4 \pm 0.1$
March 2008	$1.9 \pm 0.4 \times 10^{-6}$	$-3.5 \pm 0.2$
April 2008	$2.1 \pm 0.4 \times 10^{-6}$	$-3.3 \pm 0.2$
April-May 2005 + January-April 2006	$1.8 \pm 0.3 \times 10^{-6}$	$-4.2 \pm 0.3$

**Table 1.** The  $F_0$  and  $\Gamma$  during MAGIC current observations and previous observation.

$\frac{dN}{dE} = F_0 \left( \frac{E}{200 \text{ GeV}} \right)^\Gamma \text{ m}^{-2} \text{ s}^{-1} \text{ TeV}^{-1}$ , where  $F_0$  is normalization flux at 200 GeV and  $\Gamma$  is photon index during our observation, which are given in Table 1. The values obtained during our previous observations (Albert et al. 2007) are also given.

The interaction of VHE  $\gamma$ -rays with the extragalactic background light (EBL; a recent review can be found in Mazin & Raue 2007), leads to attenuation of the VHE  $\gamma$ -ray flux via  $e^+e^-$  pair production. We computed the deabsorbed (i.e., intrinsic) fluxes using a specific ‘low star formation model’ of the EBL (Kneiske et al. 2004), assuming a source redshift of  $z = 0.3$ . The resulting deabsorbed points are represented as empty squares in Fig.1.

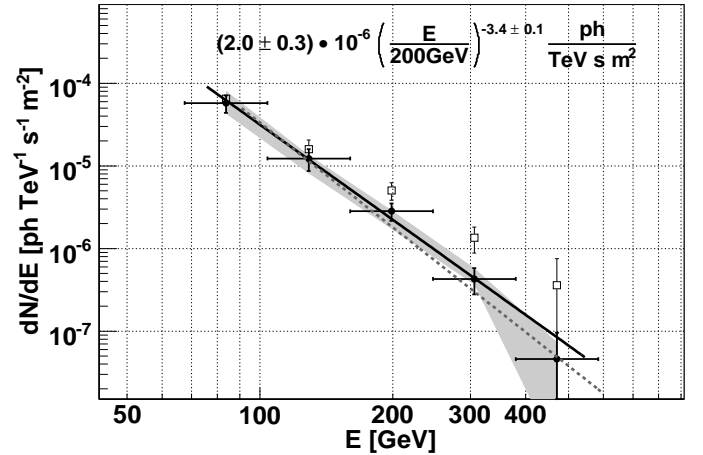


**Fig. 1.** The MAGIC measured spectrum of PG 1553+113 (filled circles). The  $\chi^2/\text{DOF}$  of the fit is 1.36/3. The EBL-corrected points are shown as empty squares. The spectrum obtained during our first observation is shown in dashed line.

The HE data reduction results from AGILE are summarized in Table 2. The  $2\sigma$  upper limits obtained by AGILE are consistent with the average flux point observed by the *Fermi*-LAT for this source during August-October 2008 (Abdo et al. 2009). The upper limit obtained in the third time interval has been used for the modeling of SED. The fluxes and corresponding effective photon frequencies of the other telescopes which contribute to this multi-frequency campaign are reported in Table 3.

The SED of PG 1553+113 is shown in Fig.2. The VHE and HE  $\gamma$ -ray flux points are from MAGIC and AGILE respectively. The X-ray point, provided by RXTE/ASM, represents the average flux between March 1 and May 31, 2008. The optical R-band point, provided by the KVA telescope, is the average flux obtained on March 18 and 19. The flux provided by Abastumani is the average flux of April 1 - May 17 observations. In addition to these data, we also used the NIR flux from REM. To assess

Time interval	Energy	U.L.Flux [ $\text{ph m}^{-2}\text{s}^{-1}$ ]
March 16-21	$> 100 \text{ MeV}$	$5.6 \times 10^{-3}$
	$> 200 \text{ MeV}$	$3.6 \times 10^{-3}$
March 25-30	$> 100 \text{ MeV}$	$5.5 \times 10^{-3}$
	$> 200 \text{ MeV}$	$2.8 \times 10^{-3}$
April 10-30	$> 100 \text{ MeV}$	$3.4 \times 10^{-3}$
	$> 200 \text{ MeV}$	$2.1 \times 10^{-3}$

**Table 2.**  $2\sigma$  Upper limit calculated from AGILE data in three different time intervals.

the soundness of this addition, we checked the optical variability of the source during this period using Abastumani data, and found that the source was essentially stable (minimum and maximum values of  $\log(\nu F_\nu)$  are  $-10.14$  and  $-10.02$  respectively). For comparison of the HE flux, we included the flux points from the *Fermi*  $\gamma$ -ray Space Telescope (Flux,  $F(E > 100 \text{ MeV}) = 8 \pm 1 \times 10^{-4} \text{ ph m}^{-2} \text{ s}^{-1}$  and photon index,  $\Gamma = 1.7 \pm 0.6$ ; Abdo et al. 2009). The average flux (15–30 keV) obtained from the X-ray satellite *Swift*/BAT during 39 months (December 2004 - February 2008) of observation (Cusumano et al. 2009) is also included.

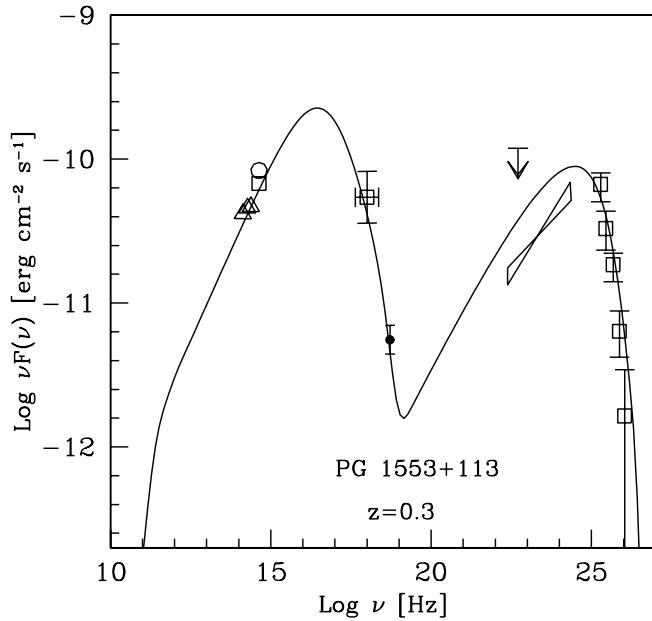


**Fig. 2.** The average SED of PG 1553+113 measured in March-April 2008. The empty triangles denote the REM data, the open square represents the KVA data, the open circle denotes the Abastumani data, and the open square denotes RXTE/ASM data. The arrow at HE denotes the AGILE upper limit. The empty squares in VHE range are the deabsorbed MAGIC data. We also show the non-simultaneous flux points from *Fermi* (bowtie) and *Swift*/BAT (small filled circle).

We fit the resulting simultaneous SED with a homogeneous one-zone SSC model (Tavecchio et al. 2001). The model assumes that the source is a spherical plasmon of radius  $R$ , moving with a Doppler factor  $\delta$  towards the observer at an angle  $\theta$  with respect to the line of sight threaded with a uniforming distributed tangled magnetic field of strength  $B$ . The injected relativistic par-

ticle population is described as a broken power-law spectrum with normalization  $K$ , extending from  $\gamma_{\min}$  to  $\gamma_{\max}$  with indices  $n_1$  and  $n_2$  below and above the break Lorentz factor  $\gamma_{\text{br}}$ . By fitting the observed flux with the model, we obtain following parameters:  $\gamma_{\min} = 1$ ,  $\gamma_{\text{br}} = 3 \times 10^4$ ,  $\gamma_{\max} = 2 \times 10^5$ ,  $K = 0.5 \times 10^4 \text{ cm}^{-3}$ ,  $n_1 = 2$ ,  $n_2 = 4.7$ ,  $B = 0.7 \text{ G}$ ,  $R = 1.3 \times 10^{16} \text{ cm}$ , and  $\delta = 23$ . The optical and X-ray flux constrain on the slope of electron energy distribution (EED), while X-ray and VHE spectrum fix the Lorentz factors.

The difference between the current SED and the previous one published in Albert et al. (2007) is due to flux variation in the X-ray and small variation of the slope of VHE spectrum. We used different SED models in the current and previous paper. Doppler factor (21 and 23 respectively) and the size of emission region ( $1.3 \times 10^{16}$  and  $1.16 \times 10^{16}$  respectively) are comparable, while the magnetic field is 0.7 G in both cases. The major difference in SED is arising from the difference in EED.

Instrument	$\log(\nu [\text{Hz}])$	$\log(\nu F(\nu)) [\text{erg cm}^{-2} \text{s}^{-1}]$
KVA	14.63	-10.17
Abastumani	14.63	-10.08
REM	14.38	-10.33
	14.27	-10.34
	14.13	-10.38
XTE	18.03	-10.3

**Table 3.** Effective frequencies, and corresponding fluxes from PG 1553+113 from KVA, Abastumani, REM and RXTE instruments obtained during this campaign.

During this campaign, no significant variability of VHE flux is found. The integral flux ( $E > 200 \text{ GeV}$ ) during these observations is  $1.3 \pm 0.3 \times 10^{-7} \text{ cm}^{-2} \text{s}^{-1}$  while during the first observations that was  $1.0 \pm 0.4 \times 10^{-7} \text{ cm}^{-2} \text{s}^{-1}$ . The X-ray flux<sup>2</sup> increases by about a factor of two, while the averaged X-ray flux during 39 months of *Swift*/BAT observation agrees with our SED. Optical flux during our first observation and current observation does not show any significant variability. The *Fermi* bowtie and lowest-energy MAGIC data points together with the model fit indicate a variability at HE or VHE  $\gamma$ -rays.

Our results suggest that the variability of PG 1553+113 at different frequencies is time dependent: hence, only a simultaneous multi-frequency monitoring campaign over a large time span will give more information on the source. Relative to this fact, it is worth mentioning that the AGILE and MAGIC data presented here constitute the first simultaneous broad-band  $\gamma$ -ray observation (and ensuing SED) of any blazar, though the first simultaneous detection accomplished during the multi-frequency campaign of Mkn 421 (Donnarumma et al. 2009), and the first broad-band  $\gamma$ -ray spectrum was obtained from PKS 2155-304 (Aharonian et al. 2009) by HESS and *Fermi*.

**Acknowledgements.** The MAGIC collaboration would like to thank the Instituto de Astrofísica de Canarias for the excellent working condition at the Observatorio del Roque de los Muchachos at La Palma. Major support from Germany's Bundesministerium für Bildung, Wissenschaft, Forschung und Technologie and Max-Planck-Gesellschaft, Italy's Istituto Nazionale di Fisica Nucleare (INFN) and Istituto Nazionale di Astrofisica (INAF), and Spain's Ministerio de Ciencia e Innovación is gratefully acknowledged. The work was also supported by Switzerland's ETH Research grant TH34/043, Poland's Ministertwo Nauki i Szkolnictwa Wyższego grant N N203 390834, and Germany's Young Investigator Program of the Helmholtz Gemeinschaft.

<sup>2</sup> Note that the X-ray data used in Albert et al. (2007) was not taken simultaneously with VHE and optical data.

This work was also supported by Georgian National Science Foundation grant GNSF/ST07/4-180. EP acknowledges support from the Italian Space Agency through grants ASI-INAF I/023/05/0 and ASI I/088/06/0.

## References

- Abdo, A.A. et al. 2009, *ApJ*, 700, 597  
 Aharonian, F.A. et al. 2006, *A&A*, 448, 19  
 Aharonian, F.A. et al. 2008, *A&A*, 477, 481  
 Aharonian, F.A. et al. 2009, *Astrophys. J.*, 696, 150  
 Albert, J. et al. 2007, *A&A*, 654, 119  
 Albert, J. et al. 2008a, *ApJ*, 674, 1037  
 Albert, J. et al. 2008b, *Nucl. Instr. Meth. A*, 588, 424  
 Albert, J. et al. 2009, *A&A*, 493, 467  
 Aliu, E. et al. 2009, *Astropart. Phys.*, 30, 293  
 Baixeras, C. et al. 2004, *Nuclear Instruments and methods in Physics Research A*, 518, 188  
 Blandford, R.D. & Znajek, R.L. 1997, *MNRAS*, 179, 433  
 Bretz, T. et al. 2005, *Proc. 29th ICRC*, 4, 315  
 Bretz, T. & Dorner, D. 2008, *AIP Conf. Proc.*, 1085, 664  
 Cortina, J. et al. 2005, *Proc. 29th ICRC*, 5, 359  
 Covino, S. et al. 2001, *ASP Conference Series*, Vol. TBD  
 Cusumano, G. et al. 2009, To be published in *A&A* [arXiv:0906.4788]  
 Dermer, C. D. & Schlickeiser, A. 1993, *ApJ*, 416, 458  
 Dolcini, A. et al. 2005, *A&A*, 443, 33  
 Donnarumma, I. et al. 2009, *Astrophys. J.*, 691, 13  
 Dorner, D. et al. 2005, *Proc. 29th ICRC*, 5, 175  
 Dorner, D. et al. 2009, *A&A* arXiv:0808.0279  
 Falomo, R. & Treves, A. 1990, *PASP*, 102, 1120  
 Feroci, M. et al. 2007, *Nucl. Instrum. Methods Phys. Res. A*, 581, 728  
 Fomin, V.P. et al. 1994, *Astropart. Physics*, 2, 137  
 Fiorucci, M. & Tosti, G. 1996, *A&AS*, 116, 403  
 Fiorucci, M. et al. 1998, *PASP*, 110, 105  
 Goebel, F. et al. 2005, *Proc. 29th ICRC*, 5, 179  
 Goebel, F. et al. 2007, *Proc. 30th ICRC*, 3, 1481  
 Hillas, A.M. et al. 1985, *Proc. 19th ICRC*, 3, 445  
 Kneiske, T.M. et al. 2004, *A&A*, 413, 807  
 Levine, A.M. et al. 1996, *ApJ*, 469, L33  
 Maraschi, L. Ghisellini, G. & Celotti, A. 1992, *ApJ*, 397, 5  
 Mazin, D. & Goebel, F. 2007, *ApJ Letters*, 655, 13  
 Mazin, D. & Raue, M. 2007, *A&A*, 471, 439  
 Monet, D. et al. 1998, The PMM USNO-A2.0 Catalog  
 (<http://adsabs.harvard.edu/abs/1998USNO2.C.....0M>)  
 Riegel, B. & Bretz, T. 2005, *Proc. 29th ICRC*, 5, 215  
 Riegel, B. et al. 2005, *Proc. 29th ICRC*, 5, 219  
 Sbarufatti, B. et al. 2006, *ApJ*, 132, 1  
 Schlegel, D.J. 1998, *ApJ*, 500, 525  
 Sikora, M. et al. 1994, *ApJ*, 421, 153  
 Urry, C.M. & Padovani, P. 1995, *PASP*, 107, 803  
 Tavani, M. et al. 2009, *A&A*, 502, 995  
 Treves, A. et al. 2007, *A&A*, 473, 17  
 Tavecchio, F. et al. 2001, *ApJ*, 554, 725  
 Vercellone, S. et al. 2008, *ApJL*, 676, 13  
 Villata, M. et al. 1998, *A&AS*, 130, 305
- <sup>1</sup> IFAE, Edifici Cn., Campus UAB, E-08193 Bellaterra, Spain  
<sup>2</sup> ETH Zurich, CH-8093 Switzerland  
<sup>3</sup> INAF National Institute for Astrophysics, I-00136 Rome, Italy  
<sup>4</sup> Universidad Complutense, E-28040 Madrid, Spain  
<sup>5</sup> Technische Universität Dortmund, D-44221 Dortmund, Germany  
<sup>6</sup> Universitat Autònoma de Barcelona, E-08193 Bellaterra, Spain  
<sup>7</sup> Università di Padova and INFN, I-35131 Padova, Italy  
<sup>8</sup> Inst. de Astrofísica de Canarias, E-38200 La Laguna, Tenerife, Spain  
<sup>9</sup> University of Łódź, PL-90236 Lodz, Poland  
<sup>10</sup> Tuorla Observatory, University of Turku, FI-21500 Piikkiö, Finland  
<sup>11</sup> Deutsches Elektronen-Synchrotron (DESY), D-15738 Zeuthen, Germany  
<sup>12</sup> Max-Planck-Institut für Physik, D-80805 München, Germany  
<sup>13</sup> Università di Siena, and INFN Pisa, I-53100 Siena, Italy  
<sup>14</sup> Universitat de Barcelona (ICC/IEEC), E-08028 Barcelona, Spain  
<sup>15</sup> Universität Würzburg, D-97074 Würzburg, Germany  
<sup>16</sup> Depto. de Astrofísica, Universidad, E-38206 La Laguna, Tenerife, Spain  
<sup>17</sup> Università di Udine, and INFN Trieste, I-33100 Udine, Italy
- <sup>18</sup> Institut de Ciències de l'Espai (IEEC-CSIC), E-08193 Bellaterra, Spain  
<sup>19</sup> Inst. de Astrofísica de Andalucía (CSIC), E-18080 Granada, Spain  
<sup>20</sup> Croatian MAGIC Consortium, Institute R. Boskovic, University of Rijeka and University of Split, HR-10000 Zagreb, Croatia  
<sup>21</sup> University of California, Davis, CA-95616-8677, USA  
<sup>22</sup> Inst. for Nucl. Research and Nucl. Energy, BG-1784 Sofia, Bulgaria  
<sup>23</sup> INAF/Osservatorio Astronomico and INFN, I-34143 Trieste, Italy  
<sup>24</sup> ICREA, E-08010 Barcelona, Spain  
<sup>25</sup> Università di Pisa, and INFN Pisa, I-56126 Pisa, Italy  
<sup>26</sup> supported by INFN Padova  
<sup>27</sup> now at: Centro de Investigaciones Energéticas, Medioambientales y Tecnológicas (CIEMAT), Madrid, Spain  
<sup>28</sup> now at: Max-Planck-Institut für Kernphysik, D-69029 Heidelberg, Germany  
<sup>29</sup> deceased  
<sup>30</sup> INAF/IASF-Bologna, I-40129 Bologna, Italy  
<sup>31</sup> INAF/IASF-Roma, I-00133 Roma, Italy  
<sup>32</sup> INAF, Astronomical Obs. Brera, I-23807 Merate, Italy  
<sup>33</sup> INAF, Trieste Astronomical Observatory, I-34143 Trieste, Italy  
<sup>34</sup> INAF, Astronomical Obs. Torino, I-10025 Torino, Italy  
<sup>35</sup> University of Perugia, I-06123 Perugia, Italy  
<sup>36</sup> University of Insubria, I-22100 Como, Italy  
<sup>37</sup> INAF, IASF-Milano, I-20133 Milano, Italy  
<sup>38</sup> Abastumani Astrophysical Observatory, 383762 Abastumani, Georgia  
<sup>39</sup> now at: Scuola Normale Superiore, I-56126 Pisa, Italy